Pharmaceutical Sciences and Drug Design
ISSN: 3062-4428
2022, Volume 2, Page No: 117-129

Available online at: www.galaxypub.co/page/journals

Galaxy Publication

Galaxy Publication

Perillaldehyde Inhibits Colorectal Cancer by Targeting SRD5A1 to Induce Autophagy via Suppression of the PI3K/AKT Pathway

Daniel Rivera[1]*, Isaac Kelly[1]

[1]Department of Phytochemistry, Faculty of Pharmaceutical Sciences, University of Tokyo, Tokyo, Japan.

***E-mail** ✉ daniel.rivera.jp@gmail.com

Received: 26 January 2022; **Revised:** 10 March 2022; **Accepted:** 11 March 2022

ABSTRACT

Colorectal cancer (CRC) ranks as the third most prevalent malignancy worldwide, and effective treatment options remain limited. Perillaldehyde (PAH), a key bioactive component derived from Perilla, has shown promise in managing CRC, yet its underlying mechanisms are not fully understood. This work investigates the anti-CRC potential of PAH and elucidates its mode of action, aiming to support its development as a candidate therapeutic agent. For the in vitro portion, we employed CCK-8 assays, colony formation tests, EdU incorporation, flow cytometry, and Western blot analyses to examine how PAH influences CRC cell growth and apoptosis. For in vivo evaluation, we created a subcutaneous xenograft mouse model to determine PAH's antitumor effects. Transcriptome sequencing was conducted to uncover possible mechanisms—particularly those related to autophagy—and these findings were further confirmed by TEM, immunofluorescence, Western blotting, and inhibitor-based experiments. SRD5A1 was identified through Swiss Target Prediction as a likely target and validated via molecular docking, molecular dynamics simulations, and CETSA. Subsequent bioinformatics analyses explored the clinical importance and functional relevance of SRD5A1, and a selective inhibitor was used for experimental confirmation.

PAH displayed notable anti-CRC activity in both cellular and animal models. RNA-seq results, supported by follow-up experiments, indicate that PAH may suppress CRC by activating autophagy through modulation of the PI3K/AKT pathway. Computational and experimental data suggest SRD5A1 as a potential PAH target, where PAH treatment reduces SRD5A1 expression and enhances autophagic signaling via PI3K/AKT inhibition. PAH appears to exert its anti-CRC effects partly by interacting with SRD5A1, subsequently promoting autophagy through suppression of the PI3K/AKT pathway. These findings offer new insights into possible diagnostic and therapeutic approaches for CRC.

Keywords: Perillaldehyde, Colorectal cancer, Autophagy, PI3K/AKT pathway, SRD5A1

How to Cite This Article: Rivera D, Kelly I. Perillaldehyde Inhibits Colorectal Cancer by Targeting SRD5A1 to Induce Autophagy via Suppression of the PI3K/AKT Pathway. Pharm Sci Drug Des. 2022;2:117-29. https://doi.org/10.51847/QT3T9FNSaT

Introduction

CRC is among the most frequent malignant tumors of the digestive system. Its global incidence and fatality rates continue to rise, contributing to 9.2% of all cancer-related deaths each year [1]. Projections anticipate that CRC cases will increase to 2.5 million by 2035 [2]. Besides hereditary susceptibility, lifestyle-related factors—including unhealthy diet, tobacco use, obesity, and limited physical activity—play key roles in CRC onset [3–5]. In clinical practice, standard therapies rely on surgical procedures, radiotherapy, and chemotherapy [6]. However, additional options that offer higher efficacy and safety are urgently required.

The PI3K/AKT cascade is a major oncogenic signaling route involved in numerous human cancers [7]. This pathway regulates essential tumor characteristics such as cell proliferation, survival, metabolism, and metastasis. Aberrant PI3K/AKT signaling is frequently observed in CRC, with PIK3CA mutations—affecting the catalytic PI3K subunit p110α—detected in 10–15% of cases [8]. Such alterations lead to continuous AKT activation, fostering resistance to apoptosis and excessive tumor growth. Moreover, PI3K/AKT interacts with other cancer-related pathways, including Wnt/β-catenin, intensifying malignant transformation. This signaling axis also

contributes to angiogenesis, immune evasion, metastatic behavior, and alterations in the tumor microenvironment [9]. Consequently, understanding how to regulate and therapeutically target the PI3K/AKT pathway is essential for the advancement of CRC treatment strategies.

Autophagy, a conserved cellular degradation process, is involved in a broad spectrum of physiological and disease-related events [10, 11]. It displays a dual nature in oncology, participating in both tumor promotion and tumor suppression [12]. In CRC, autophagy affects genomic stability, the apoptotic machinery, inflammatory responses, and immune modulation—all of which are intimately tied to disease progression [13]. The PI3K/AKT pathway is recognized as a major autophagy-inhibiting mechanism [14]. Enhancing autophagy to trigger apoptotic death has emerged as a viable anticancer strategy [15]. The development of small-molecule therapeutics that target autophagic pathways is therefore considered a promising avenue for CRC management.

SRD5A1, the enzyme known as steroid 5-alpha reductase type I, participates in steroid processing and helps regulate circulating sex hormones. Elevated SRD5A1 expression has been documented in multiple malignancies—breast, prostate, and non-small-cell lung cancers among them—raising the possibility that it contributes to oncogenic behavior. Recent reports have pointed to SRD5A1 as a gene that may promote CRC development and suggested it could serve as a new biomarker [9]. Through our bioinformatic screening, SRD5A1 emerged as a probable binding or regulatory target of PAH. Additional studies indicate that SRD5A1 can influence essential tumor-related functions—cell proliferation, programmed cell death, and autophagy—by interacting with the PI3K/AKT pathway. Even so, its exact function in colorectal cancer is still not clearly determined, and small-molecule inhibitors directed at SRD5A1 have not yet been tested in CRC. Taking all of this into account, we proposed that PAH might reduce CRC progression by interfering with SRD5A1, and this study was designed to examine that possibility.

Extracts from perilla possess numerous biological activities [16], largely attributed to PAH, a major monoterpene and essential oil component. PAH has been described as anti-inflammatory, antioxidative, antifungal, anticancer, vasodilatory, anti-atherosclerotic, lipid-lowering, and capable of slowing cell-cycle progression [17–21], Nevertheless, how PAH influences CRC on a mechanistic level has not been resolved.

Here, we investigated PAH's antitumor potential in CRC using both in vitro and in vivo methods. Our findings indicate that PAH enhances autophagic activity in CRC cells through PI3K/AKT modulation. We additionally identified SRD5A1 as a possible molecular target of PAH. These observations expand current knowledge regarding PAH as an anti-CRC compound and support further structure-based optimization.

Materials and Methods

Cell lines and culture

Human colon epithelial cells (NCM460) and CRC cell lines (HCT116 and SW480) were obtained from Shanghai East Hospital. HCT116 and SW480 cells were maintained in DMEM (Gibco, USA) containing 10% FBS and 1% penicillin-streptomycin, while NCM460 cells were grown in RPMI-1640 (Gibco, USA). All cultures were kept at 37°C with 5% CO_2.

Cell viability assay

PAH (CAS 18031-40-8) was purchased from MCE (New Jersey, USA) and dissolved to 400 mM in DMSO. Cells were seeded in 96-well plates at 2×10^3 cells/well, then exposed to PAH concentrations of 0, 50, 100, 200, or 400 μM for 24 or 48 hours. Viability was assessed using a CCK-8 kit (Beyotime, Shanghai, China): 10 μL of reagent was added to each well and incubated for 2 hours at 37°C before measuring absorbance at 450 nm. GraphPad Prism 9.0 was used to calculate IC_{50} values. Each condition included five wells (n = 5) and was repeated in three independent experiments (n = 3).

Colony formation assay

HCT116 and SW480 cells were seeded at 1×10^3 cells/well into 6-well plates. Once attached, cells received PAH at 0, 100, or 200 μM for 24 hours, and colonies were allowed to form for 7–10 days. Fixation was performed using 4% paraformaldehyde for 20 minutes, followed by staining with 0.1% crystal violet for 15 minutes. Colonies were enumerated with ImageJ. Experiments were conducted three times independently (n = 3).

EdU-DNA synthesis assay

Proliferation was evaluated using the BeyoClick™ EdU-488 kit (Beyotime, Shanghai, China). After 24 hours of PAH treatment, cells were incubated with 10 μM EdU for 2 hours, counterstained with Hoechst 33342 for 10 minutes, and imaged using a Leica confocal microscope. All assays were repeated three times (n = 3).

Flow cytometry

Apoptotic responses to PAH were measured using the Annexin V-FITC/PI apoptosis kit (MultiSciences, Hangzhou, China). HCT116 and SW480 cells were plated at 1×10^3 cells/well in 6-well plates and treated with 0, 100, or 200 μM PAH for 24 hours. Staining was performed following the manufacturer's instructions, and samples were evaluated using a BD FACSAria II cytometer. All experiments were independently repeated three times (n = 3).

Western blot (WB)

Cells were harvested using a scraper after being rinsed twice with ice-cold PBS. Lysis was performed with RIPA buffer supplemented with 2% protease and phosphatase inhibitors (Beyotime, Shanghai, China). Protein concentration was determined using a BCA assay kit (Beyotime, Shanghai, China). Extracted proteins were separated by SDS-PAGE and transferred onto PVDF membranes. Membranes were blocked for 1 hour with 5% skim milk, followed by overnight incubation with primary antibodies at room temperature. Secondary antibody incubation was performed the following day. Protein signals were visualized using the Super Sensitive ECL kit (Meilunbio, Dalian, China). Antibodies included: Bax (1:1000, ZEN-BIOSCIENCE, #380709), Bcl-2 (1:1000, ZEN-BIOSCIENCE, #381702), PI3 Kinase p85α (1:1000, Abcam, ab182651), p-PI3 Kinase p85α (1:1000, ZEN-BIOSCIENCE, #341468), AKT (1:2000, Proteintech, #10176-2-AP), p-AKT (Ser 473) (1:1000, ZEN-BIOSCIENCE, #381555), SQSTM1/p62 (1:1000, ZEN-BIOSCIENCE, #380612), LC3B (1:1000, ZEN-BIOSCIENCE, #382687), SRD5A1 (1:1000, Proteintech, #66329-1-Ig), and GAPDH (1:10000, Proteintech, #60004-1-Ig). All WB experiments were performed three independent times (n = 3).

Immunofluorescence (IF) analysis

Cells were seeded on confocal dishes and treated with different PAH concentrations. After fixation in 4% paraformaldehyde for 20 minutes, permeabilization was carried out using 0.3% Triton X-100 (Beyotime, Shanghai, China). Cells were then blocked for 10 minutes with QuickBlock™ Immuno Staining Block Solution (Beyotime, Shanghai, China). LC3B primary antibody exposure took place overnight at 4°C, followed by a 1-hour dark incubation with an Alexa Fluor 488 conjugated secondary antibody (Beyotime, Shanghai, China). Nuclei were counterstained using DAPI, and a fluorescence quencher (Beyotime, Shanghai, China) was applied before laser confocal imaging. Each IF assay was repeated three times independently (n = 3).

RNA-Seq

Total RNA was isolated with TRIzol after treating HCT116 cells for 24 hours with PAH at 0, 100, or 200 μM. Sequencing libraries were constructed and analyzed on the Illumina NovaSeq6000, generating 150-bp paired-end reads. All sequencing experiments were performed in triplicate (n = 3).

Molecular docking

The three-dimensional structure of PAH was obtained from the AlphaFold Protein Structure Database. Docking was conducted using AutoDock 1.5.7, and molecular interactions were visualized via PyMOL 2.5.4.

Molecular dynamics simulation

Simulations began with the top docking conformation and were run using GROMACS V2020.3, applying the AMBER99SB force field and SPC/E water model; sodium ions were added for neutralization. Energy minimization used both steepest-descent and conjugate-gradient methods. Systems were equilibrated at 300 K under NVT conditions for 2000 ps, followed by 2000 ps in NPT. A 50-ns production run was performed, collecting coordinates every 10 ps. Stability was evaluated through RMSD measurements.

Bioinformatics analysis

Differential expression of genes between normal tissue and colon adenocarcinoma (COAD) was examined using GEPIA2, applying $|Log2FC| \geq 1$ and $p = 0.01$ as screening criteria. TCGA normal datasets were integrated with GTEx controls for comparison.

Animal experiment

A total of eighteen male NXG immunodeficient mice (6–8 weeks old) were purchased from Changzhou Cavens Animal Experiment Company. All animal procedures followed the Xiamen University Ethics Committee guidelines (approval XMULAC20240001). Each mouse received a subcutaneous injection of 1×10^7 HCT116 cells. Animals were randomly assigned to three groups and orally administered PAH at 100 mg/kg or 200 mg/kg daily for 21 consecutive days once tumor size reached the required threshold. Tumor volume and body weight were recorded every 3 days. After the treatment period, mice were sacrificed and tumors were excised, photographed, and fixed in 4% paraformaldehyde for further analyses.

HE staining

Tumor samples preserved in paraffin were sectioned into 4-μm slices. These were processed using a hematoxylin–eosin staining kit from Beyotime (Shanghai, China), and the stained slides were subsequently evaluated with a Motic EasyScan system (Xiamen, China).

Immunohistochemistry (IHC)

For IHC, paraffin sections underwent deparaffinization and hydration, followed by antigen retrieval in citrate buffer (pH 6.0). The slides were then kept at 4°C overnight with primary antibodies targeting Ki67 and PCNA. Afterward, an HRP-conjugated secondary antibody was applied for 1 hour, and color development was performed using the DAB method.

Statistical analysis

All numerical data were processed with GraphPad Prism 9.0 and are presented as the mean ± SD. For comparisons between two groups, an independent t-test was used, whereas datasets involving more than two groups were examined using one-way ANOVA. Differences were considered significant when $p < 0.05$. Significance levels were labeled as follows:

*p < 0.05, **p < 0.01, ***p < 0.001, ****p < 0.0001.

Results and Discussion

PAH restrains CRC cell proliferation

To preliminarily evaluate the impact of PAH, a 24-hour CCK-8 assay was conducted across multiple concentrations **(Figure 1a)**. As illustrated in **Figure 1b**, PAH caused a dose-responsive decline in CRC cell viability. The IC50 values were 239.4 μM in HCT116 cells and 218.9 μM in SW480 cells. Normal NCM460 cells, however, exhibited minimal toxicity at 200 μM PAH, with an IC50 of 576.9 μM, suggesting selectivity for malignant cells. Colony formation assays and EdU incorporation studies further demonstrated obvious reductions in colony counts and EdU-positive nuclei after 24 hours of exposure in SW480 and HCT116 **(Figures 1c and 1d)**.

And because of the impact on mothers' mental health due to pregnancy-related complications, pregnant mothers are reluctant to have sex with their spouses.

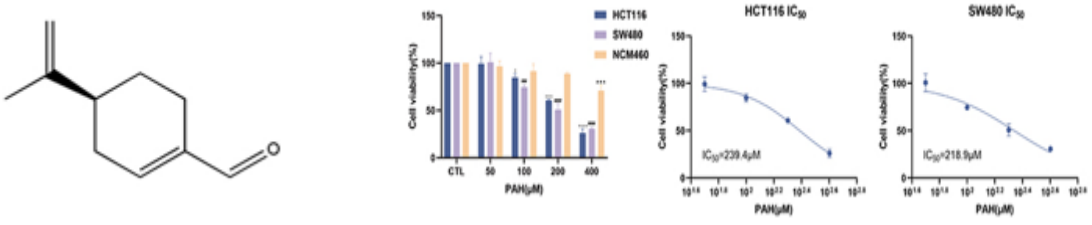

a) b)

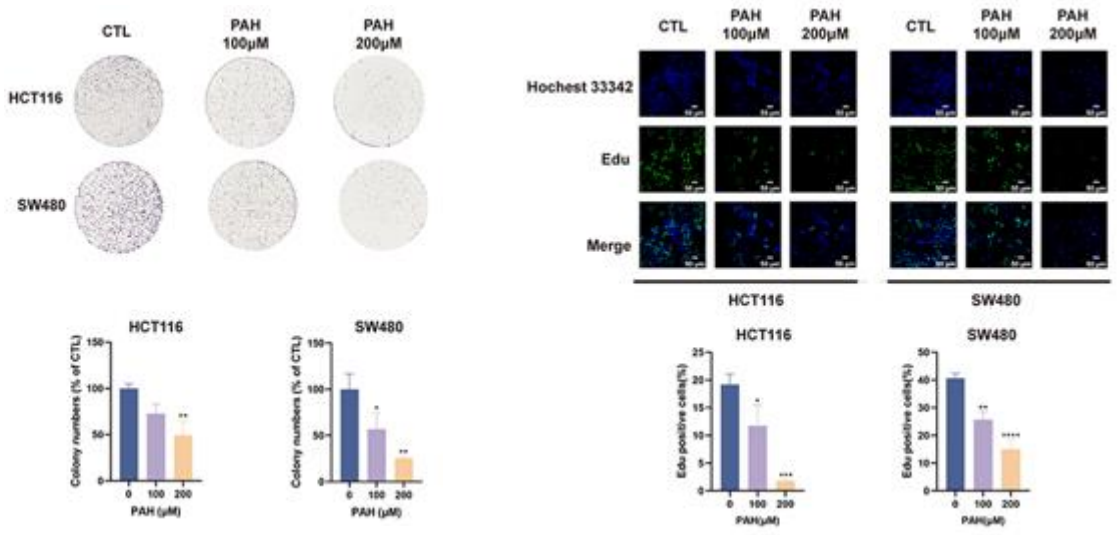

c) d)

Figure 1. displays: (a) PAH chemical structure; (b) CCK-8 viability results; (c) colony assays at the indicated PAH doses; (d) EdU staining at various concentrations for 24 h (scale bar: 50 μm). Values represent mean ± SD, with significance thresholds as stated: *p < 0.05, **p < 0.01, ***p < 0.001, ****p < 0.0001.

PAH promotes apoptotic cell death in CRC

We next investigated whether PAH induces apoptosis in CRC lines. Annexin V/PI staining analyzed by flow cytometry revealed a clear dose-dependent increase in apoptotic fractions following 24-hour treatment **(Figure 2a)**. Western blotting further showed suppressed Bcl-2 levels and elevated BAX expression after PAH administration **(Figure 2b)**.

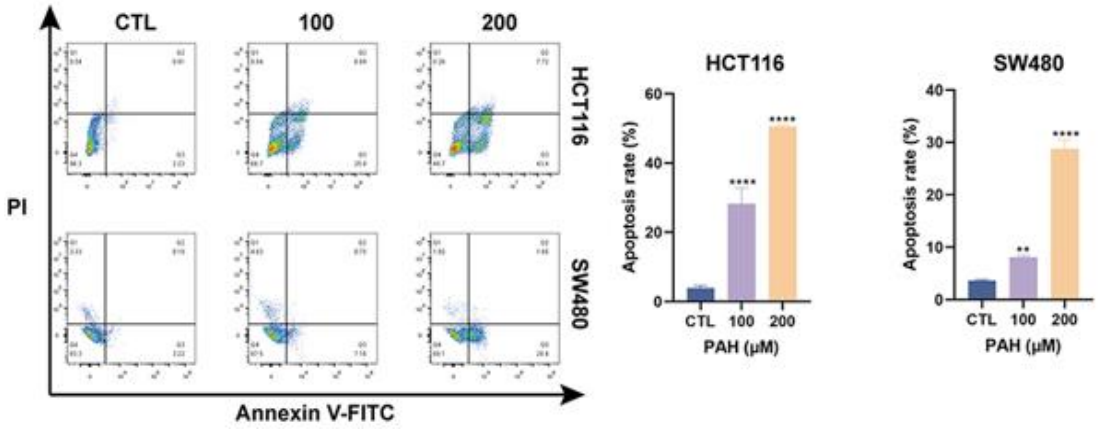

a)

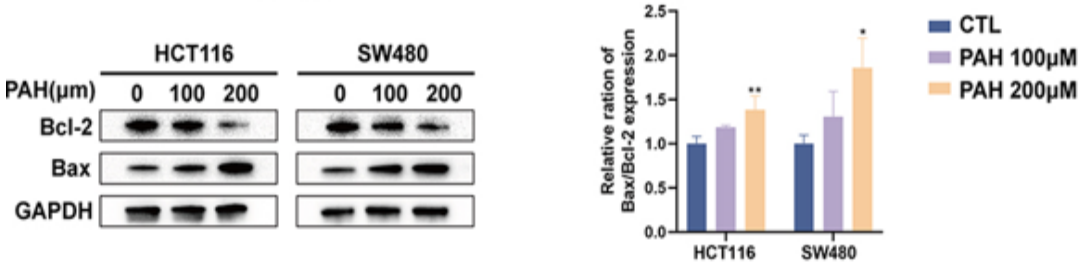

b)

Figure 2. summarizes (a) apoptotic percentages measured by Annexin V-FITC/PI and (b) changes in Bcl-2 and BAX proteins. Data are presented as mean ± SD, with significant differences marked as *p < 0.05, **p < 0.01, ****p < 0.0001.

PAH slows tumor development in CRC xenografts

To determine in vivo efficacy, HCT116 xenograft-bearing mice received oral doses of PAH at 100 mg/kg or 200 mg/kg. Throughout the treatment timeline, both PAH groups exhibited a pronounced suppression of tumor expansion relative to controls **(Figures 3a, 3b and 3d)**. Body weight remained stable with no observable harmful effects **(Figure 3c)**. Histological examination by HE staining revealed lower cell density and disrupted architecture in treated tumors **(Figure 3e)**. Immunohistochemical detection of Ki67 and PCNA showed weakened expression in the PAH-treated groups **(Figure 3f)**.

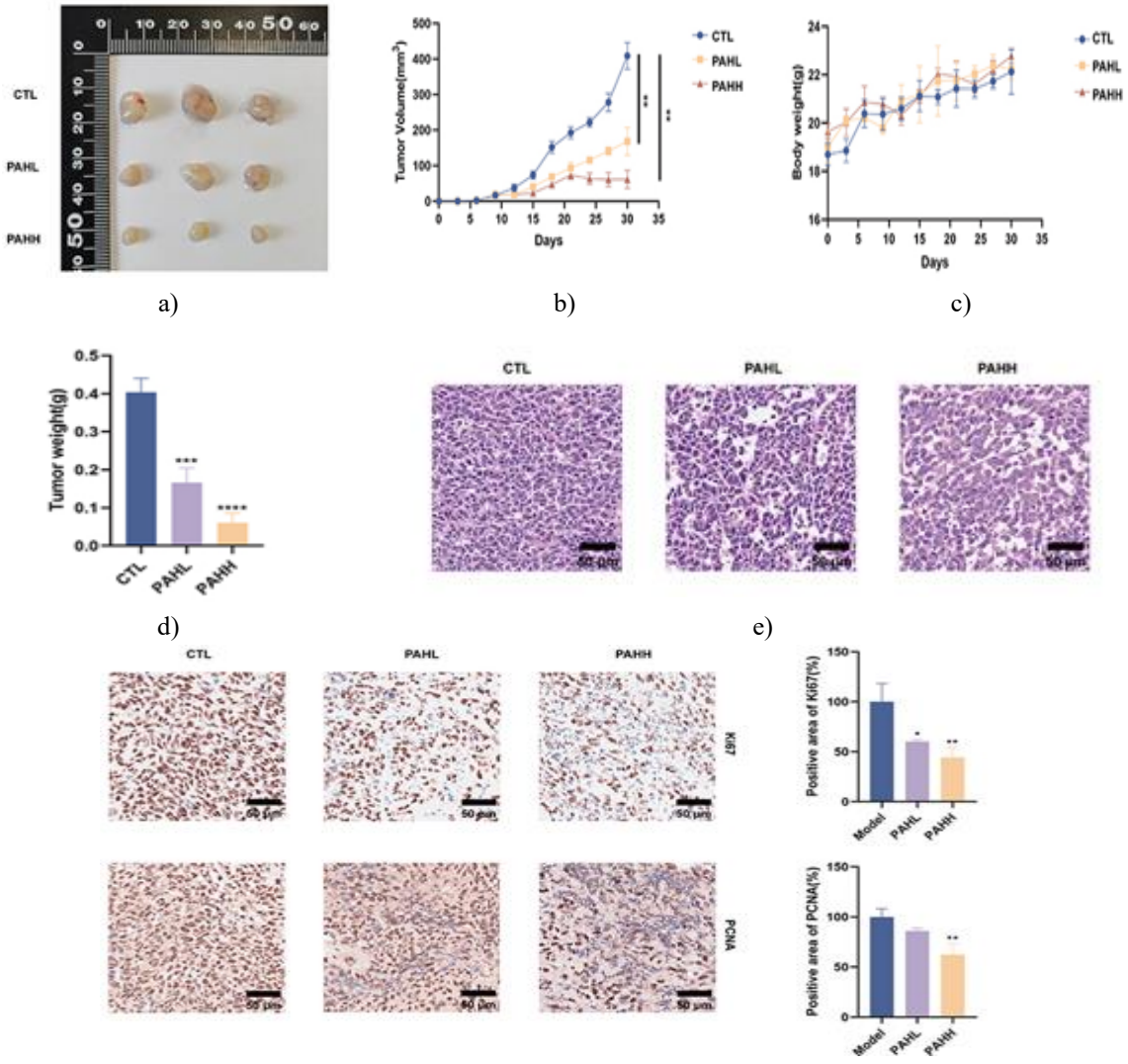

a) b) c) d) e) f)

Figure 3. Suppression of CRC Growth by PAH in Mouse Xenografts

(a) Photographs of excised tumors from animals receiving either vehicle or PAH.

(b) Plot illustrating tumor volume changes throughout the observation period.

(c) Body-weight tracking for each treatment arm.

(d) Distribution of tumor masses at the endpoint.

(e) Histological sections of representative tumors processed with HE staining.

(f) IHC micrographs visualizing Ki67 and PCNA labeling.

Quantitative values are shown as mean ± SD, with significance indicated as: *P < 0.05; **P < 0.01; ***P < 0.001; ****P < 0.0001.

RNA-Seq profiling suggests pathways influenced by PAH

Transcriptomic sequencing was performed on HCT116 cells exposed to PAH for 24 hours to explore pathways potentially underlying its anti-CRC activity. KEGG enrichment pointed toward ferroptosis, p53, and PI3K/AKT

involvement **(Figure 4a)**. In parallel, GSEA highlighted autophagy-related gene signatures as markedly altered by PAH **(Figures 4b and 4c)**.

To validate functional relevance, ferrostatin-1 (1 μM), Pifithrin-α (20 μM), or chloroquine (10 μM) were administered together with PAH **(Figure 4d)**. The ferroptosis and p53 inhibitors produced minimal impact, whereas blocking autophagy clearly mitigated PAH's inhibitory effect on CRC cell viability.

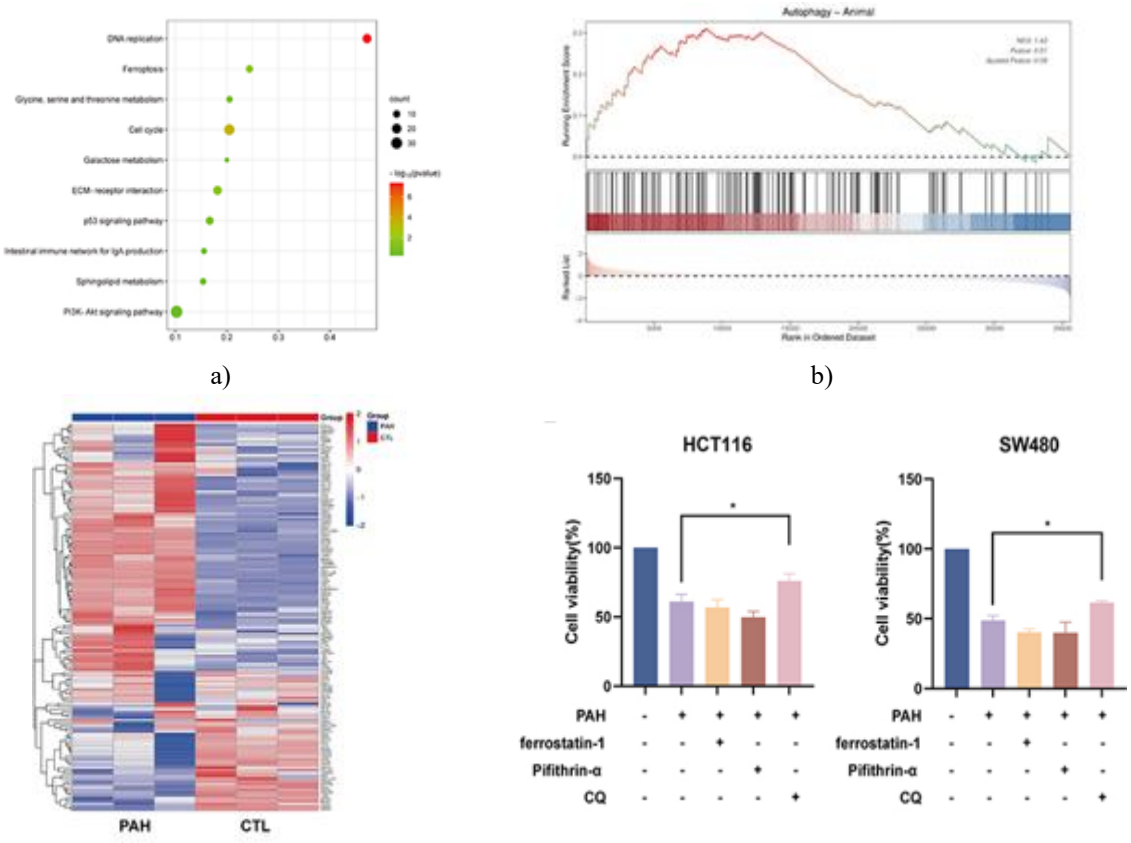

a) b) c) d)

Figure 4. (a) KEGG pathway enrichment results. (b) GSEA output. (c) Autophagy-associated expression heatmap. (d) CCK-8 viability after 24-hour co-treatments. Data presented as mean ± SD. *P < 0.05.

PAH elicits autophagy in CRC models

Ultrastructural evaluation by TEM confirmed the presence of autophagic vacuoles in SW480 and HCT116 cells following PAH exposure **(Figure 5a)**. Immunoblotting revealed dose-responsive elevation of LC3B-II accompanied by P62 reduction **(Figure 5b)**. IF staining further demonstrated amplified LC3B puncta across increasing PAH levels **(Figure 5c)**.

When cells received both PAH and the autophagy blocker chloroquine (CQ), an enhanced buildup of LC3B-II and P62 was observed, indicating intensified autophagic accumulation **(Figure 5d)**.

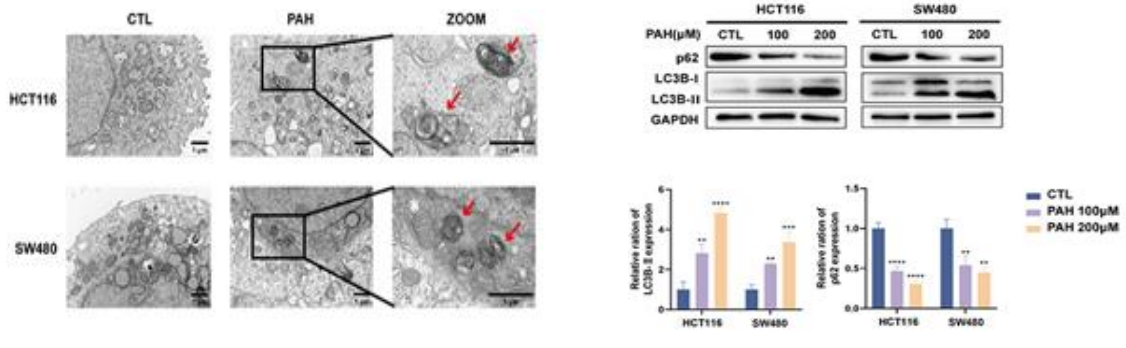

a) b)

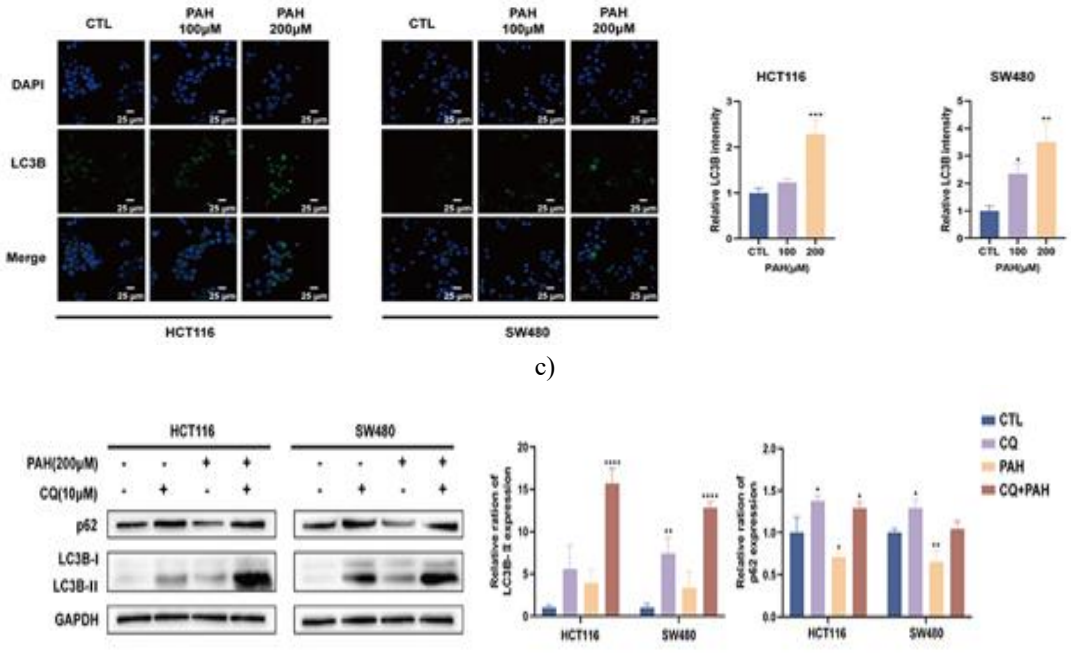

Figure 5. (a) TEM images showing autophagic vacuoles after 200 μM PAH (red arrows).
(b) LC3B and P62 expression shifts across PAH concentrations.
(c) IF pattern of LC3B puncta after 24 hours of treatment.
(d) LC3 and P62 changes with PAH + CQ (10 μM).
Values shown as mean ± SD, with *P < 0.05; **P < 0.01; ***P < 0.001; ****P < 0.0001.

PAH regulates autophagy through PI3K/AKT signaling

Expression of PI3K, AKT, and their phosphorylated forms was examined to determine involvement of this pathway. Escalating doses of PAH produced corresponding increases in p-PI3K/PI3K and p-AKT/AKT ratios **(Figure 6a)**.

In contrast, non-cancerous NCM460 cells—characterized by modest baseline PI3K/AKT activity and low SRD5A1 levels—responded to 200 μM PAH primarily with a limited, protective autophagy rather than overt autophagic cell death.

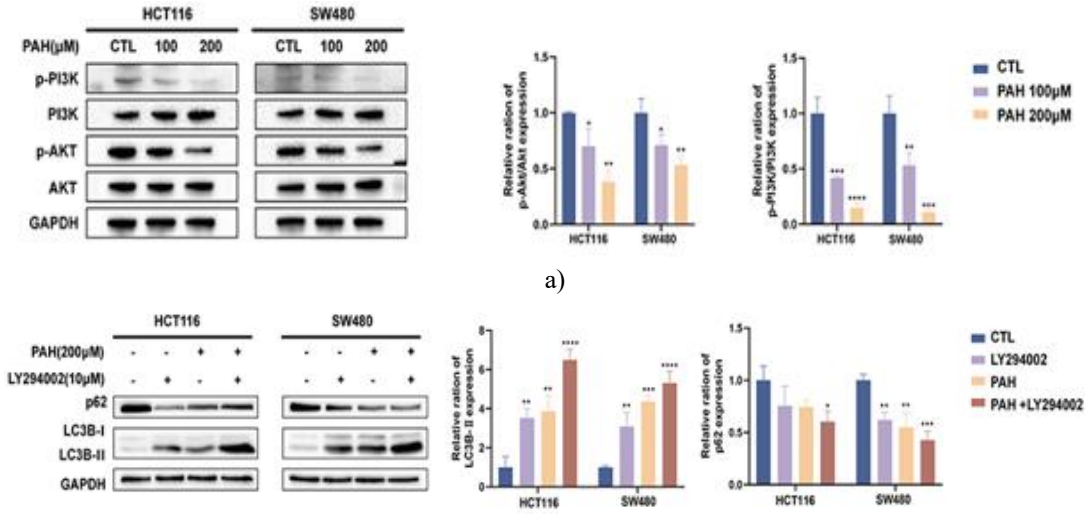

Figure 6. (a) Western blot analysis of PI3K, p-PI3K, AKT, and p-AKT under varied PAH concentrations.
(b) LC3 and P62 protein levels following PAH in combination with 10 μM LY294002.
All data are reported as mean ± SD, significance: *P < 0.05; **P < 0.01; ***P < 0.001; ****P < 0.0001.

Silencing PTEN via siRNA substantially reduced PAH-evoked autophagy, reflected by decreased LC3B-II, and also weakened PAH's cytotoxic impact as measured by CCK-8.

Conversely, chemical interruption of PI3K/AKT signaling—either via LY294002 **(Figure 6b)** or the AKT inhibitor MK-2206—enhanced PAH-associated autophagic flux, demonstrated by elevated LC3B-II and suppressed P62 levels.

PAH targets SRD5A1 to promote autophagy via the PI3K/AKT pathway

To identify the molecular targets potentially influenced by PAH, the SwissTargetPrediction platform was utilized. As shown in **Figure 7a**, SRD5A1 emerged as the top predicted target with the highest likelihood score. Molecular docking was then applied to forecast the interaction pattern between PAH and its candidate proteins [22]. Docking results indicated that PAH engages SRD5A1 through hydrogen bonds formed with HIS-94, ARG-98, and GLU-202, producing a binding energy of −5.7 kcal/mol—evidence of a strong binding propensity **(Figure 7b)**. These findings were further supported by molecular dynamics simulations **(Figure 7c)**. RMSD, a metric for evaluating complex stability, showed an average deviation below 0.4 nm, with oscillations stabilizing to less than 0.2 nm after 30 ns, confirming both system steadiness and docking reliability [23].

To test whether PAH's anticancer function relies on SRD5A1 modulation, CRC cells were treated with PAH and analyzed via WB. As depicted in **Figure 7d**, SRD5A1 protein abundance was markedly diminished following treatment. Additional verification using CETSA demonstrated that PAH increased the thermal resilience of the SRD5A1 complex in both HCT116 and SW480 cells compared with untreated controls **(Figure 7e)**. Prior evidence has connected high SRD5A1 expression with tumor progression across different malignancies. We next evaluated SRD5A1 expression in cancer versus matched non-tumor tissues across TCGA datasets. **Figure 7f** indicates that SRD5A1 is significantly elevated in many tumor types, particularly in COAD and READ. A comparison between CRC samples (n = 275) and normal tissues (n = 349) revealed a pronounced increase in SRD5A1 among CRC cases **(Figure 7g)**. Moreover, ROC analysis showed that SRD5A1 possesses strong diagnostic accuracy for CRC **(Figure 7h)**.

To further explore how PAH influences CRC biology via SRD5A1, we analyzed the GSE147456 dataset from GEO, which contrasts transcriptomes of HCT116 cells with SRD5A1 knockdown against controls. The enrichment outcomes suggested that PAH may affect CRC partly by regulating the PI3K/AKT cascade **(Figure 7i)**. Earlier studies have noted that SRD5A1 suppression in multiple myeloma can dampen PI3K/AKT signaling and enhance autophagy, thereby restraining tumor development [24]. To corroborate these findings, cells were exposed to dutasteride, a known SRD5A1 inhibitor. WB assays showed that co-treatment with dutasteride reduced PI3K/AKT pathway activity while enhancing autophagy-related markers, ultimately facilitating autophagy induction **(Figures 7j and 7k)**.

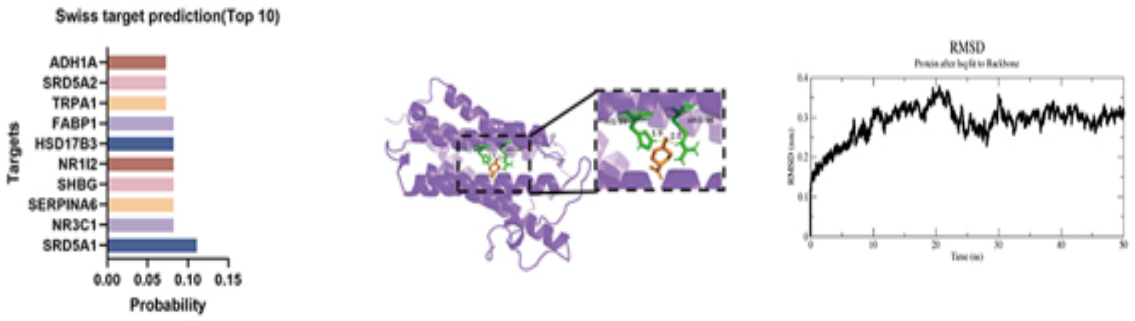

a) b) c)

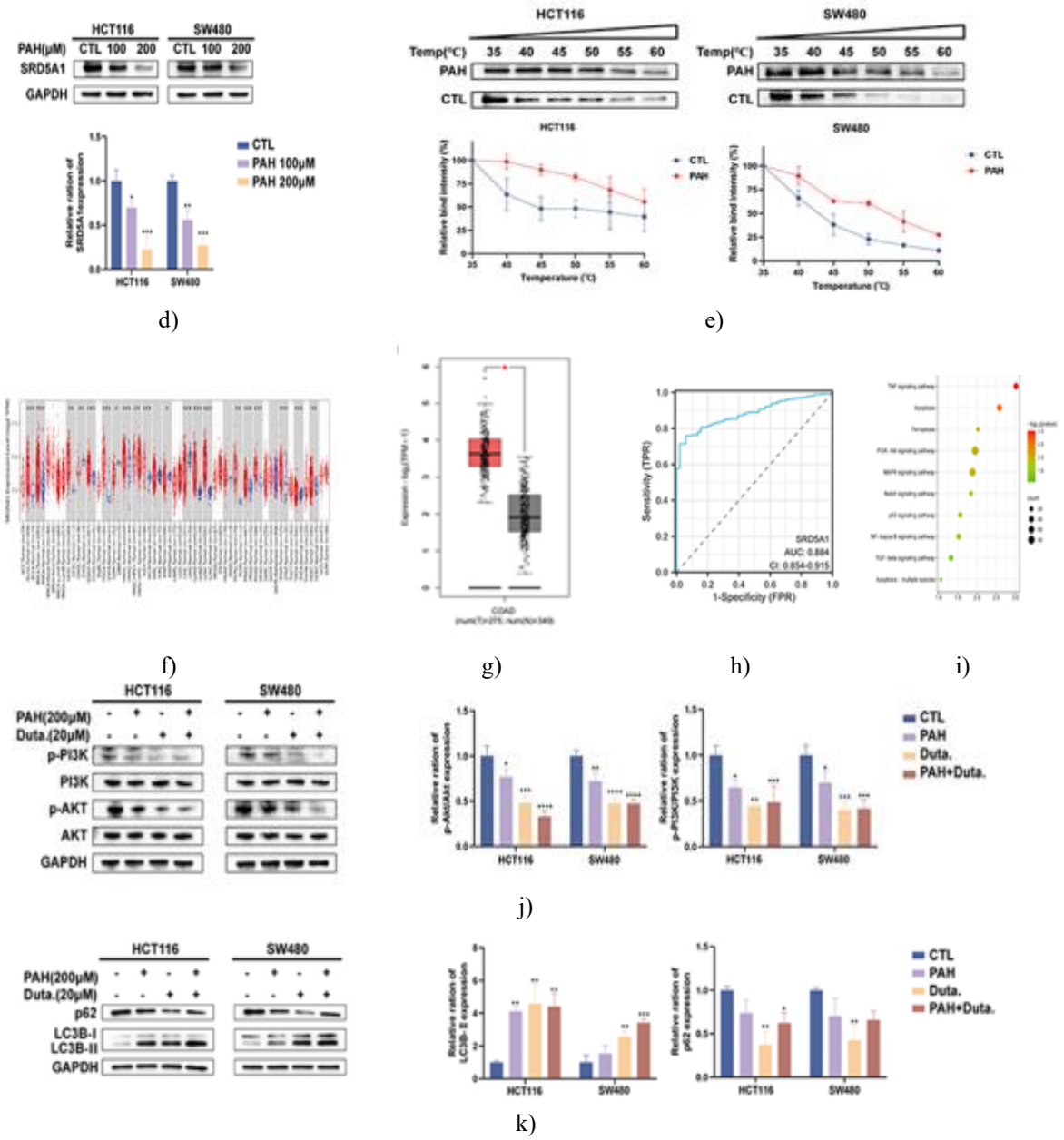

Figure 7. The potential PAH-associated targets. (a) SwissTargetPrediction lists the ten most probable PAH-binding proteins. (b) Computational modeling illustrates predicted PAH–SRD5A1 interactions. (c) MD simulation metrics for the PAH–SRD5A1 complex. (d) WB analysis of SRD5A1 expression. (e) CETSA assesses SRD5A1 thermal stability in PAH-treated HCT116 and SW480 cells. (f) TCGA-based comparison of SRD5A1 expression across cancers. (g) GEPIA2 comparison of SRD5A1 expression between tumor (T) and normal (N) tissues in COAD. (h) Diagnostic ROC assessment. (i) KEGG pathway enrichment from GSE147456. (j) Levels of AKT, p-AKT, PI3K, and p-PI3K after PAH exposure with/without dutasteride (20 μM). (k) Evaluation of LC3 and p62 following combined PAH and dutasteride (20 μM) treatment. Data are mean ± SD. *P < 0.05, **P < 0.01, ***P < 0.001, ****P < 0.0001.

This study focused on PAH, a major constituent of perilla essential oil and a volatile monoterpene recognized for its low toxicity and approved safety status by both the US FDA and the Flavor and Extract Manufacturers Association [25]. Prior work by Zhang *et al.* [26] demonstrated that PAH suppresses gastric cancer via autophagy activation. Lin *et al.* additionally showed its capacity to counter prostate cancer progression and influence stemness. Catanzaro *et al.* [27] further linked PAH to anti-leukemic effects through ferroptosis. Building on these findings, our work confirms that PAH exerts notable anti-CRC activity, supporting its potential as a viable therapeutic agent.

Our findings reveal that PAH markedly inhibits CRC cell proliferation and promotes apoptosis. Importantly, PAH doses up to 200 μM produced minimal toxicity toward the normal epithelial cell line NCM460. This selectivity aligns with earlier reports showing preferential PAH cytotoxicity toward malignant cells [28, 29]. In our viability assays, the IC50 for NCM460 was approximately 576.9 μM—much higher than IC50 values obtained for CRC cell lines HCT116 (239.4 μM) and SW480 (218.9 μM). These results indicate that PAH can effectively impair tumor cells at concentrations well below the toxicity threshold for normal epithelium.

To better clarify how PAH contributes to CRC suppression, transcriptome-based analyses were conducted to predict its functional actions. KEGG enrichment revealed PAH's association with several pathways, including ferroptosis and p53. Although the autophagy pathway showed relatively low enrichment in KEGG, GSEA pointed to autophagy as a major contributor to PAH's therapeutic influence on CRC. Experiments combining PAH with pathway-specific inhibitors demonstrated that blocking autophagy eliminated PAH's ability to reduce CRC cell growth. Autophagy, a conserved mechanism of intracellular degradation in eukaryotic cells [30], involves the merging of autophagosomes with lysosomes to form autolysosomes, which remove damaged cellular components and help maintain homeostasis and renewal [31]. Considering the dualistic role of autophagy in cancer, enhancing this process has emerged as a compelling approach in CRC treatment. In our analyses, PAH markedly increased LC3B fluorescence and elevated autophagic flux. Chloroquine (CQ), which halts autophagy at a late step by preventing autophagosome–lysosome fusion [32], was used to assess flux. Cells exposed to PAH displayed higher autophagic activity relative to CQ alone, indicating that PAH both activates autophagy and facilitates autophagosome degradation. Multiple molecular systems influence autophagy, with the PI3K/AKT pathway functioning as a central regulator. Further examination confirmed that PI3K/AKT is a principal pathway targeted by PAH. Western blot data revealed that PAH sharply reduced phosphorylation of both PI3K and AKT. When combined with LY294002, a PI3K inhibitor, autophagy-related proteins were further elevated, supporting the view that PAH promotes autophagy by downregulating PI3K/AKT. Besides LY294002, additional inhibitors (such as MK-2206) and suppressive elements (including PTEN) within the PI3K/AKT axis can generate comparable outcomes.

We then used bioinformatic analysis to propose that PAH's anticancer actions arise from its interaction with and inhibition of SRD5A1, followed by preliminary experimental confirmation. SRD5A1 is primarily found in the skin [33] and has been linked to several cancers [24, 34–36]. Wei *et al.* [35] showed that SRD5A1 affects CRC cell growth and promotes apoptosis, identifying it as a viable diagnostic and prognostic indicator for CRC. Our findings demonstrate that PAH suppresses SRD5A1, interferes with the PI3K/AKT pathway, and activates autophagy, highlighting its therapeutic promise. Mechanistically, the PAH target SRD5A1 exhibits far lower expression in NCM460 cells relative to CRC cells, and baseline PI3K/AKT activity is also reduced. Correspondingly, PAH-induced autophagy in NCM460 is modest and largely protective, rather than leading to autophagic cell death. Taken together, these results suggest that PAH selectively targets malignant cells while exerting minimal impact on normal tissue.

When evaluating PAH as a CRC therapeutic, its functional potency is constrained by IC50 measurements of 265.0 μM in HCT116 and 240.2 μM in SW480. To overcome these limitations and enhance effectiveness, PAH can serve as a scaffold for structural optimization and the development of stronger analogs. The 1,2-epoxy derivative of PAH synthesized by Andrade demonstrated substantially greater cytotoxicity toward CRC cells, with an IC50 of 16.14 μM in HCT116. This improvement indicates that adding an epoxy moiety to PAH may significantly increase its bioactivity [37].

Conclusion

In summary, our research shows that PAH inhibits colorectal cancer development by targeting SRD5A1, resulting in reduced PI3K/AKT signaling and activation of autophagy. Both in vivo and in vitro results confirmed its anti-proliferative and pro-apoptotic actions. Bioinformatic evaluations further revealed that SRD5A1 is markedly elevated in CRC tissues, and ROC analysis demonstrated substantial diagnostic potential. Altogether, these data support PAH as a compelling therapeutic candidate for CRC and identify SRD5A1 as both a treatment target and a diagnostic biomarker.

Acknowledgments: None

Conflict of Interest: None

Financial Support: None

Ethics Statement: None

References

1. Dekker E, Tanis PJ, Vleugels JLA, Kasi PM, Wallace MB. Colorectal cancer. Lancet. 2019;394(10207):1467–80. doi:10.1016/S0140-6736(19)32319-0
2. Bray F, Ferlay J, Soerjomataram I, Siegel RL, Torre LA, Jemal A. Global cancer statistics 2018: GLOBOCAN estimates of incidence and mortality worldwide for 36 cancers in 185 countries. CA Cancer J Clin. 2018;68:394–424. doi:10.3322/caac.21492
3. Murphy N, Moreno V, Hughes DJ, Vodicka L, Vodicka P, Aglago EK, et al. Lifestyle and dietary environmental factors in colorectal cancer susceptibility. Mol Aspects Med. 2019;69:2–9. doi:10.1016/j.mam.2019.06.005
4. Keum N, Giovannucci E. Global burden of colorectal cancer: emerging trends, risk factors and prevention strategies. Nat Rev Gastroenterol Hepatol. 2019;16(12):713–32. doi:10.1038/s41575-019-0189-8
5. Yang L, Atakhanova N, Arellano MT, Mohamed MY, Hani T, Fahdil AA, et al. Translational research of new developments in targeted therapy of colorectal cancer. Pathol Res Pract. 2023;252:154888. doi:10.1016/j.prp.2023.154888
6. Johdi NA, Sukor NF, Hu L, Qiu L, Zhu L. Colorectal Cancer Immunotherapy: options and Strategies. Front Immunol. 2020;11:11. doi:10.3389/fimmu.2020.00011
7. He Y, Sun MM, Zhang GG, Yang J, Chen KS, Xu WW, et al. Targeting PI3K/Akt signal transduction for cancer therapy. Signal Transduct Target Ther. 2021;6(1):425. doi:10.1038/s41392-021-00828-5
8. Danielsen SA, Eide PW, Nesbakken A, Guren T, Leithe E, Lothe RA. Portrait of the PI3K/AKT pathway in colorectal cancer. Biochimica Et Biophysica Acta. 2015;1855(1):104–21.
9. Świechowski R, Pietrzak J, Wosiak A, Mik M, Balcerczak E. Genetic Insights into colorectal cancer: evaluating PI3K/AKT signaling pathway genes expression. Int J Mol Sci. 2024;25(11):5806. doi:10.3390/ijms25115806
10. Levine B, Kroemer G. Autophagy in the pathogenesis of Disease. Cell. 2008;132(1):27–42. doi:10.1016/j.cell.2007.12.018
11. Zhang Y, Li H, Lv L, Lu K, Li H, Zhang W, et al. Autophagy: dual roles and perspective for clinical treatment of colorectal cancer. Biochimie. 2023;206:49–60. doi:10.1016/j.biochi.2022.10.004
12. Kimmelman AC. The dynamic nature of autophagy in cancer. Genes Dev. 2011;25(19):1999–2010. doi:10.1101/gad.17558811
13. Qian Q, Zhou H, Chen Y, Shen C, He S, Zhao H, et al. VMP1 related autophagy and apoptosis in colorectal cancer cells: VMP1 regulates cell death. Biochem Biophys Res Commun. 2014;443(3):1041–7. doi:10.1016/j.bbrc.2013.12.090
14. Zhong J, Ding S, Zhang X, Di W, Wang X, Zhang H, et al. To investigate the occurrence and development of colorectal cancer based on the PI3K/AKT/mTOR signaling pathway. Front Biosci. 2023;28(2):37. doi:10.31083/j.fbl2802037
15. Galluzzi L, Pietrocola F, Bravo-San Pedro JM, Amaravadi RK, Baehrecke EH, Cecconi F, et al. Autophagy in malignant transformation and cancer progression. EMBO J. 2015;34(7):856–80. doi:10.15252/embj.201490784
16. Wu X, Dong S, Chen H, Guo M, Sun Z, Luo H. Perilla frutescens: a traditional medicine and food homologous plant. Chin Herb Med. 2023;15(3):369–75. doi:10.1016/j.chmed.2023.03.002
17. Lin Z, Huang S, LingHu X, Wang Y, Wang B, Zhong S, et al. Perillaldehyde inhibits bone metastasis and receptor activator of nuclear factor-κB ligand (RANKL) signaling-induced osteoclastogenesis in prostate cancer cell lines. Bioengineered. 2022;13(2):2710–9. doi:10.1080/21655979.2021.2001237
18. Elegbede JA, Flores R, Wang RC. Perillyl alcohol and perillaldehyde induced cell cycle arrest and cell death in BroTo and A549 cells cultured in vitro. Life Sci. 2003;73(22):2831–40. doi:10.1016/S0024-3205(03)00701-X

19. Uemura T, Yashiro T, Oda R, Shioya N, Nakajima T, Hachisu M, et al. Intestinal anti-inflammatory activity of perillaldehyde. J Agric Food Chem. 2018;66(13):3443–8. doi:10.1021/acs.jafc.8b00353
20. Chen L, Wang F, Qu S, He X, Zhu Y, Zhou Y, et al. Therapeutic potential of perillaldehyde in ameliorating vulvovaginal candidiasis by reducing vaginal oxidative stress and apoptosis. Antioxidants. 2022;11(2):178. doi:10.3390/antiox11020178
21. Chu Z, Li Y, Wang L, Wei S, Yang S, Zeng H. Perillaldehyde: a promising antibacterial agent for the treatment of pneumonia caused by Acinetobacter baumannii infection. Int Immunopharmacol. 2024;126:111311. doi:10.1016/j.intimp.2023.111311
22. Lu X, Yan G, Dawood M, Klauck SM, Sugimoto Y, Klinger A, et al. A novel moniliformin derivative as pan-inhibitor of histone deacetylases triggering apoptosis of leukemia cells. Biochem Pharmacol. 2021;194:114677. doi:10.1016/j.bcp.2021.114677
23. Qiao X, Wu X, Chen S, Niu MM, Hua H, Zhang Y. Discovery of novel and potent dual-targeting AXL/HDAC2 inhibitors for colorectal cancer treatment via structure-based pharmacophore modelling, virtual screening, and molecular docking, molecular dynamics simulation studies, and biological evaluation. J Enzyme Inhib Med Chem. 2024;39(1):2295241. doi:10.1080/14756366.2023.2295241
24. Dou R, Qian J, Wu W, Zhang Y, Yuan Y, Guo M, et al. Suppression of steroid 5alpha-reductase type I promotes cellular apoptosis and autophagy via PI3K/Akt/mTOR pathway in multiple myeloma. Cell Death Dis. 2021;12(2):206. doi:10.1038/s41419-021-03510-4
25. Tang LF, Ma X, Xie LW, Zhou H, Yu J, Wang ZX, et al. Perillaldehyde mitigates ionizing radiation-induced intestinal injury by inhibiting ferroptosis via the Nrf2 signaling pathway. Mol Nutr Food Res. 2023;67(19). doi:10.1002/mnfr.202300232.
26. Zhang Y, Liu S, Feng Q. Perilaldehyde activates AMP-activated protein kinase to suppress the growth of gastric cancer via induction of autophagy. J Cell Biochem. 2019;120(2):1716–25. doi:10.1002/jcb.27491
27. Hale AN, Ledbetter DJ, Gawriluk TR, Rucker, III EB. Autophagy. Autophagy. 2013;9(7):951–72. doi:10.4161/auto.24273
28. Hobbs CA, Taylor SV, Beevers C, Lloyd M, Bowen R, Lillford L, et al. Genotoxicity assessment of the flavouring agent, perillaldehyde. Food Chem Toxicol. 2016;97:232–42. doi:10.1016/j.fct.2016.08.029
29. Catanzaro E, Turrini E, Kerre T, Sioen S, Baeyens A, Guerrini A, et al. Perillaldehyde is a new ferroptosis inducer with a relevant clinical potential for acute myeloid leukemia therapy. Biomed Pharmacother. 2022;154:113662. doi:10.1016/j.biopha.2022.113662
30. Li H, Li X, Xia R, Zhang X, Jin T, Zhang H. PHGDH knockdown increases sensitivity to SR1, an aryl hydrocarbon receptor antagonist, in colorectal cancer by activating the autophagy pathway. FEBS J. 2024;291(8):1780–94.
31. Wu Z, Zhang W, Chen L, Wang T, Wang X, Shi H, et al. CDK12 inhibition upregulates ATG7 triggering autophagy via AKT/FOXO3 pathway and enhances anti-PD-1 efficacy in colorectal cancer. Pharmacol Res. 2024;201:107097. doi:10.1016/j.phrs.2024.107097
32. Kocak M, Ezazi Erdi S, Jorba G, Maestro I, Farrés J, Kirkin V, et al. Targeting autophagy in disease: established and new strategies. Autophagy. 2022;18(3):473–95. doi:10.1080/15548627.2021.1936359
33. Thigpen AE, Silver RI, Guileyardo JM, Casey ML, McConnell JD, Russell DW. Tissue distribution and ontogeny of steroid 5 alpha-reductase isozyme expression. J Clin Invest. 1993;92(2):903–10. doi:10.1172/JCI116665
34. Kapp FG, Sommer A, Kiefer T, Dölken G, Haendler B. 5-alpha-reductase type I (SRD5A1) is up-regulated in non-small cell lung cancer but does not impact proliferation, cell cycle distribution or apoptosis. Cancer Cell Int. 2012;12(1):1. doi:10.1186/1475-2867-12-1
35. Wei R, Zhong S, Qiao L, Guo M, Shao M, Wang S, et al. Steroid 5α-reductase type I induces cell viability and migration via nuclear factor-κB/vascular endothelial growth factor signaling pathway in colorectal cancer. Front Oncol. 2020;10:10. doi:10.3389/fonc.2020.00010
36. Thomas LN, Douglas RC, Rittmaster RS, Too CKL. Overexpression of 5α-reductase type 1 increases sensitivity of prostate cancer cells to low concentrations of testosterone. Prostate. 2009;69(6):595–602. doi:10.1002/pros.20911
37. Andrade LN, Severino P, Amaral RG. Evaluation of cytotoxic and antitumor activity of perillaldehyde 1,2-epoxide. J Med Plant Res. 2018;12(30):590–600. doi:10.5897/JMPR2018.6699